Signal, Image and Video Processing (2023) 17:83–89
https://doi.org/10.1007/s11760-022-02206-2

ORIGINAL PAPER

Nonorthogonal multiple access with adaptive transmit power and energy harvesting using intelligent reflecting surfaces for cognitive radio networks

Raed Alhamad[1]

Received: 29 June 2021 / Revised: 17 December 2021 / Accepted: 13 March 2022 / Published online: 4 April 2022

Abstract

In this paper, we derive the throughput of cognitive radio networks (CRN) where the secondary source S_S harvests energy and adapts its power to generate an interference at primary destination P_D less than T. S_S transmits a linear combination of symbols to K nonorthogonal multiple access (NOMA) users. Intelligent reflecting surfaces (IRS) are placed between the secondary source and NOMA users. A set I_i of reflectors of IRS is dedicated to user U_i so that all reflections are in phase at U_i. We derive the throughput at each user and the total throughput when IRS are used in CRN-NOMA. We optimize the NOMA powers as well as the harvesting duration α. When $N_i = 8, 32$ reflectors per user are employed, we obtain 24 and 41 dB gain with respect to CRN-NOMA with adaptive transmit power, energy harvesting and without IRS.

Keywords IRS · Energy harvesting · Adaptive transmit power · Cognitive radio networks

1 Introduction

Intelligent reflecting surfaces (IRS) improve the throughput of wireless systems as all reflections are in phase at the destination [1–5]. The phase shift of kth reflector depends on the phase of channel gain between the source and kth IRS reflector as well as the phase of channel gain between IRS and destination [6–8]. IRS for NOMA systems and fixed transmit power was recently analyzed in [9]. A set I_i of reflectors are dedicated to user U_i so that all reflections are in phase at U_i. In [9], there is a single network without energy harvesting and the results cannot be applied to CRN-NOMA where the secondary source harvests energy and transmits with an adaptive transmit power. IRS have been deployed to enhance the throughput of millimeter wave communications [10,11] as well as optical communications [12]. IRS with finite phase shifts were suggested in [13]. Asymptotic performance analysis of wireless networks using IRS was discussed in [14]. When the number of reflectors is doubled, a 6 dB enhancement in throughput was observed in [1,15,16].

✉ Raed Alhamad
ralhamad@seu.edu.sa

[1] Department of Computer Science, College of Computation and Informatics, Saudi Electronic University, Riyadh, Saudi Arabia

Antenna design, prototyping and experimental results of IRS were provided in [17]. Deep and machine learning algorithms were applied to wireless networks equipped with IRS [18,19].

In this paper, we suggest the use of IRS for CRN-NOMA where the secondary source S_S harvests energy from RF received signal from node A. S_S adapts its transmit power so that the interference at secondary destination is less than T. S_S transmits a linear combination of K symbols to NOMA users. A set I_i of IRS reflectors are dedicated to user U_i so that all reflections are in phase at U_i. We derive and improve the total throughput by optimizing the harvesting process and NOMA powers. When $N_i = 8, 32$ reflectors per user are employed, we obtain 24 and 41 dB gain with respect to CRN-NOMA with adaptive transmit power, energy harvesting and without IRS [20,21]. NOMA for multi-carrier code division multiple access (MC-CDMA) has been recently suggested in [22]. The results of [22] study NOMA for MC-CDMA system with fixed powers and without IRS.

Next section describes the system model. The energy harvesting process is analyzed in Sect. 3. The throughput is derived and optimized in Sect. 4. Section 5 gives the numerical results while last section concludes the paper and suggests some perspectives.

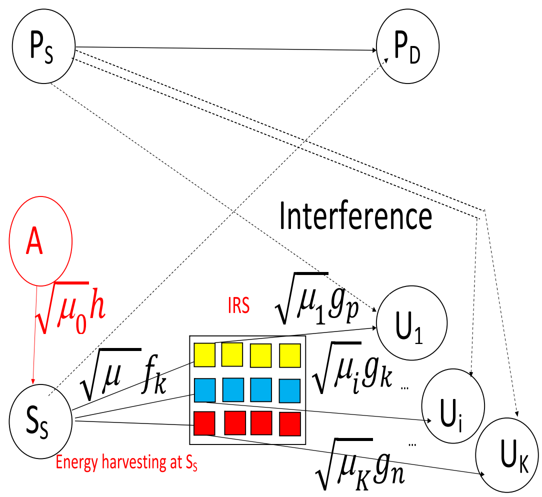

Fig. 1 IRS with adaptive transmit power and energy harvesting for NOMA systems

2 System model

Figure 1 depicts the system model containing a secondary source S_S transmitting a signal to K NOMA secondary users $U_1, U_2, \ldots, U_K$. S_S harvests energy using the received signal from node A. Then, S_S transmits a combination of K symbols to K NOMA users using an adaptive transmit power so that the generated interference at secondary destination S_D is less than threshold T. We make the analysis in the presence and absence of primary interference from primary source P_S to all users $U_i, i = 1, 2, \ldots, K$.

3 Energy harvesting model

The harvested energy at S_S is equal to [20]

$$E = P_A \alpha F \varepsilon \mu_0 |h|^2, \tag{1}$$

where F is frame duration, $0 < \alpha < 1$ is harvesting duration, P_A is the power of node A, ε is the efficiency of energy conversion and $\sqrt{\mu_0}h$ is channel gain between A and S_S and μ_0 is the average power of $\sqrt{\mu_0}h$.

The available symbol energy of S_S is written as

$$E_{s,\text{available}} = \frac{E}{(1-\alpha)\frac{F}{T_s}} = \beta |h|^2, \tag{2}$$

where

$$\beta = \frac{\mu_0 E_A \varepsilon \alpha}{1-\alpha} \tag{3}$$

where $E_A = P_A T_s$.

The adaptive symbol energy of S_S is expressed as

$$E_s = \min\left(\frac{T}{|h_{S_S P_D}|^2}, E_{s,\text{available}}\right) \tag{4}$$

where $h_{S_S P_D}$ is the channel gain between S_S and P_D. The generate interference at P_D is less than T: $E_s |h_{S_S P_D}|^2 \leq T$.

The CDF of E_s is given by

$$P_{E_s}(x) = 1 - P\left(\min\left(\frac{T}{|h_{S_S P_D}|^2}, E_{s,\text{available}}\right) > x\right) \tag{5}$$

We deduce

$$\begin{aligned} P_{E_s}(x) &= 1 - P\left(\frac{T}{|h_{S_S P_D}|^2} > x\right) P(E_{s,\text{available}} > x) \\ &= 1 - \left[1 - e^{\frac{-T}{x\rho_{S_S P_D}}}\right] e^{-\frac{x}{\beta}} \end{aligned} \tag{6}$$

where $\rho_{S_S P_D} = E(|h_{S_S P_D}|^2)$ and $E(.)$ is the expectation operator.

4 SINR and throughput analysis

4.1 Received signal model

In Fig. 1, the users are ranked as follows: U_1 is the strongest user, U_i is the ith strong user and U_K is the weakest user. The transmitted NOMA symbol by S_S is equal to

$$s = \sqrt{E_s} \sum_{i=1}^{K} \sqrt{P_i} s_i, \tag{7}$$

s_i is the symbol of user U_i and $0 < P_i < 1$ is the power allocated to U_i such that $0 < P_1 < P_2 < .. < P_K < 1$ and $\sum_{i=1}^{K} P_i = 1$.

As shown in Fig. 1, let $\sqrt{\mu} f_k$ be the channel coefficient between S_S and kth reflector of IRS where $\mu = \frac{1}{D^{ple}} = E(|\sqrt{\mu} f_k|^2)$, ple is the path loss exponent and D is the distance between S_S and IRS. Let $\sqrt{\mu_i} g_k$ be the channel coefficient between kth reflector of IRS and user U_i where $\mu_i = \frac{1}{D_i^{ple}} = E(|\sqrt{\mu_i} g_k|^2)$ and D_i is the distance between IRS and U_i. The received signal at user U_i is written as

$$r = s\sqrt{\mu}\sqrt{\mu_i} \sum_{k \in I_i} f_k g_k e^{j\theta_k} + n \tag{8}$$

where I_i is the set of reflectors dedicated to user U_i and n is a Gaussian noise with variance N_0.

θ_k is the phase shift of kth reflector given by [1]

$$\theta_k = b_k + d_k \tag{9}$$

where b_k, d_k are the phase of $f_k = a_k e^{-jb_k}$ and $g_k = c_k e^{-jd_k}$, $a_k = |f_k|$ and $c_k = |g_k|$.

Using (8) and (9), we obtain

$$r = s\sqrt{\mu}\sqrt{\mu_i}\sum_{k\in I_i} a_k c_k + n = s\sqrt{\mu}\sqrt{\mu_i}A_i + n, \tag{10}$$

where

$$A_i = \sum_{k\in I_i} a_k c_k, \tag{11}$$

We define

$$X_i = \mu\mu_i A_i^2, \tag{12}$$

Therefore, the received signal at U_i can be written as

$$r = s\sqrt{\mu}\sqrt{\mu_i}A_i + n = \sqrt{E_s X_i}\sum_{i=1}^{K}\sqrt{P_i}s_i + n$$
$$= \sqrt{Y_i}\sum_{i=1}^{K}\sqrt{P_i}s_i + n, \tag{13}$$

where

$$Y_i = E_s X_i \tag{14}$$

4.2 SINR analysis

U_i performs successive interference cancelation (SIC) and detects first s_K since $P_K > P_i, \forall i \neq K$. The corresponding SINR is

$$\Gamma^{i\to K} = \frac{Y_i P_K}{N_0 + Y_i \sum_{p=1}^{K-1} P_p} \tag{15}$$

The contribution of the detected symbol s_K is removed and U_i detects s_{K-1} with SINR

$$\Gamma^{i\to K-1} = \frac{Y_i P_{K-1}}{N_0 + Y_i \sum_{p=1}^{K-2} P_p} \tag{16}$$

The process is continued by detecting s_l for $l = K, K-1, \ldots, i$ with SINR

$$\Gamma^{i\to l} = \frac{Y_i P_l}{N_0 + Y_i \sum_{p=1}^{l-1} P_p} \tag{17}$$

There is no outage at U_i if all SINR $\Gamma^{i\to l}$ are larger than threshold x for $l = K, K-1, \ldots, i$:

$$P_{out,i}(x) = 1 - P\left(\Gamma^{i\to K} > x, \Gamma^{i\to K-1} > x, \ldots, \Gamma^{i\to i} > x\right)$$
$$= P_{Y_i}\left(\max_{i\leq l\leq K}\left(\frac{N_0 x}{P_l - x\sum_{p=1}^{l-1} P_p}\right)\right) \tag{18}$$

where $P_{Y_i}(y)$ is the CDF of Y_i provided Sect. 4.4.

The packet error probability (PEP) at U_i is deduced from the outage probability as follows [23]

$$PEP_i(\alpha, P_1, P_2, \ldots, P_K) \leq P_{out,i}(w_0), \tag{19}$$

where [23]

$$w_0 = \int_0^{+\infty} [1 - SEP(x)]^{pl} dx, \tag{20}$$

pl is packet length and $SEP(x)$ is the symbol error probability (SEP) of Q-QAM [24]

$$SEP(x) = 2\left(1 - \frac{1}{\sqrt{Q}}\right) erfc\left(\sqrt{\frac{3x}{Q-1}}\right) \tag{21}$$

The throughput at U_i is computed as

$$Thr_i(\alpha, P_1, P_2, \ldots, P_K) = (1-\alpha)log_2(Q)$$
$$\times[1 - PEP_i(\alpha, P_1, P_2, \ldots, P_K)]. \tag{22}$$

The total throughput of NOMA network is equal to

$$Thr(\alpha, P_1, P_2, \ldots, P_K) = \sum_{i=1}^{K} Thr_i(\alpha, P_1, P_2, \ldots, P_K). \tag{23}$$

We propose to optimize numerically the power allocated (OPA) to NOMA users as well as the harvesting duration α to maximize the total throughput (23):

$$Thr^{\max} = \max_{0<\alpha<1, 0<P_1<P_2<\cdots<P_K} Thr(\alpha, P_1, P_2, \ldots, P_K). \tag{24}$$

under constraint $\sum_{l=1}^{K} P_l = 1$.

4.3 Effects of primary interference

In the presence of interference from primary source P_S, the SINR at user U_i to detect s_l $l = K, K-1, \ldots, i$ becomes

$$\Gamma^{i\to l} = \frac{Y_i P_l}{N_0 + I_i + Y_i \sum_{p=1}^{l-1} P_p} \tag{25}$$

where $I_i = E_{P_S}|h_{P_S U_i}|^2$ is the interference at U_i due to the signal of P_S, E_{P_S} is the transmitted energy per symbol of P_S and $h_{P_S U_i}$ is the channel gain between P_S and U_i. For Rayleigh channels, I_i has an exponential distribution written as

$$p_{I_i}(y) = \frac{1}{\overline{I_i}} e^{-\frac{y}{\overline{I_i}}}. \quad (26)$$

where $\overline{I_i} = E(I_i)$ is the average interference at U_i.

The outage probability at U_i becomes

$$P_{out,i}(x) = \int_0^{+\infty} P_{Y_i}\left(\max_{i\le l\le K}\left(\frac{(N_0+y)x}{P_l - x\sum_{p=1}^{l-1} P_p}\right)\right) \times p_{I_i}(y)dy. \quad (27)$$

The PEP and throughput are evaluated using Eqs. (19–23).

4.4 CDF of Y_i

Let $N_i = |I_i|$ be the number of reflectors dedicated to U_i. For $N_i \ge 8$, A_i follows a Gaussian distribution with variance $\sigma^2_{A_i} = N_i(1-\frac{\pi^2}{16})$ and mean $m_{A_i} = E(A_i) = \frac{N_i \pi}{4}$.

We have

$$X_i = \mu\mu_i A_i^2, \quad (28)$$

The cumulative distribution function (CDF) of X_i is equal to

$$\begin{aligned} P_{X_i}(x) &= P(X_i \le x) = P\left(-\sqrt{\frac{x}{\mu\mu_i}} \le A_i \le \sqrt{\frac{x}{\mu\mu_i}}\right) \\ &\simeq 0.5erfc\left(\frac{-\sqrt{\frac{x}{\mu\mu_i}} - m_{A_i}}{\sqrt{2}\sigma_{A_i}}\right) \\ &\quad - 0.5erfc\left(\frac{\sqrt{\frac{N_0 x}{\mu\mu_i}} - m_{A_i}}{\sqrt{2}\sigma_{A_i}}\right) \end{aligned} \quad (29)$$

where

$$erfc(z) = \frac{2}{\sqrt{\pi}} \int_z^{+\infty} e^{-u^2} du. \quad (30)$$

By a derivative, the probability density function (PDF) of X_i is given by

$$\begin{aligned} p_{X_i}(x) &\simeq \sqrt{\frac{1}{8\pi\mu\mu_i\sigma^2_{A_i}x}} e^{-\frac{\left[\sqrt{\frac{x}{\mu\mu_i}}+m_{A_i}\right]^2}{2\sigma^2_{A_i}}} \\ &\quad + \sqrt{\frac{1}{8\pi\mu\mu_i\sigma^2_{A_i}x}} e^{-\frac{\left[\sqrt{\frac{x}{\mu\mu_i}}-m_{A_i}\right]^2}{2\sigma^2_{A_i}}}, x > 0. \end{aligned} \quad (31)$$

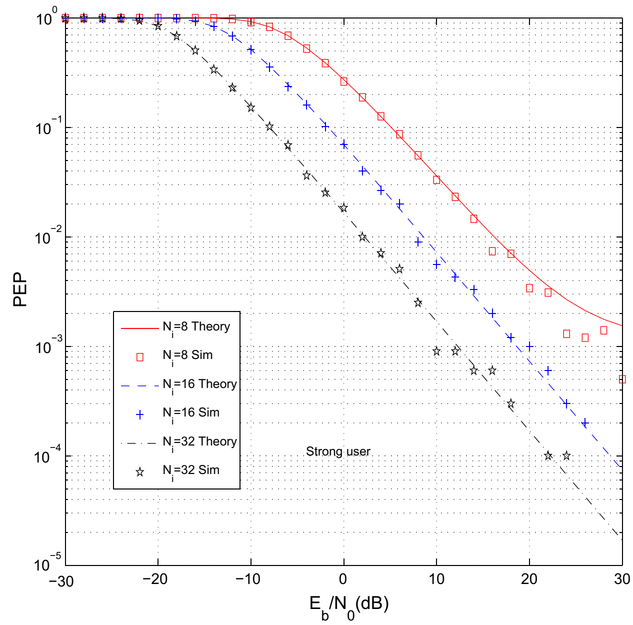

Fig. 2 PEP of strong user

The CDF of $Y_i = E_s X_i$ is evaluated as

$$P_{Y_i}(y) = \int_0^{+\infty} P_{E_s}(\frac{y}{x}) p_{X_i}(x)dx, \quad (32)$$

where $P_{E_s}(x)$ is given in (6) and $p_{X_i}(x)$ is provided in (31).

5 Numerical results

Figures 2 and 3 show the PEP at strong and weak users for $P_A = 1$, $\mu_0 = 1$, $\varepsilon = 0.5$, $K = 2$, $D = 1.5$, $D_1 = 1$, $D_2 = 1.5$, $P_1 = 0.3$, $P_2 = 0.7$, $ple = 3$, $pl = 300$ and harvesting duration $\alpha = 0.5$. The interference threshold is $T = 1$, the distance between S_S and P_D is 1.5 and the distance between primary source and users U_1 and U_2 are 2 and 2.5. These results correspond to 16 QAM modulation. The number of reflectors per user is $N_1 = N_2 = 8, 16, 32$. We observe that the PEP decreases as the number of reflectors per user N_1 and N_2 increases.

Figures 4 and 5 depict the throughput at strong and weak users for the same parameters as Figs. 2 and 3. We notice that the throughput increases as the number of reflectors increases $N_1 = N_2 = 8, 16, 32$. Besides, the simulation results are close to theoretical derivations (22). Figure 6 depicts the total throughput as the sum of throughput of strong and weak users. Harvesting duration optimization allows significant throughput enhancement.

Figure 7 depicts the total throughput in the presence of $K = 3$ NOMA users for $D_1 = 1$, $D_2 = 1.5$, $D_3 = 1.8$. The allocated powers are $P_1 = 0.2$, $P_2 = 0.3$ and $P_3 = 0.5$.

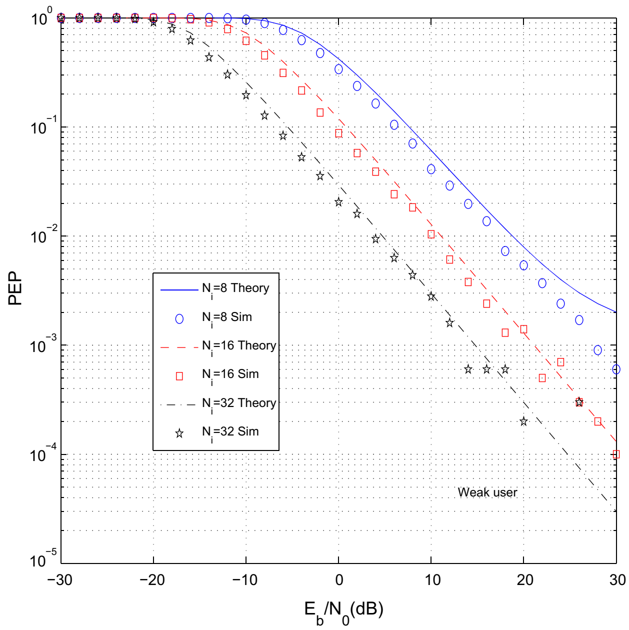

Fig. 3 PEP of weak user

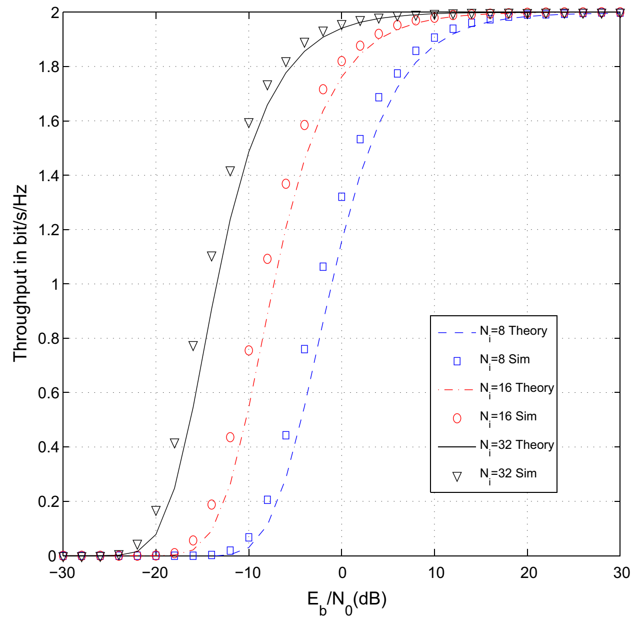

Fig. 5 Throughput at weak user

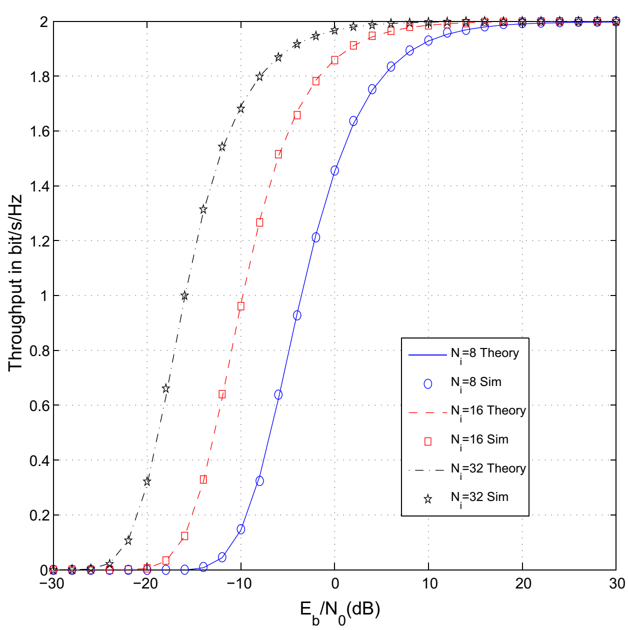

Fig. 4 Throughput at strong user

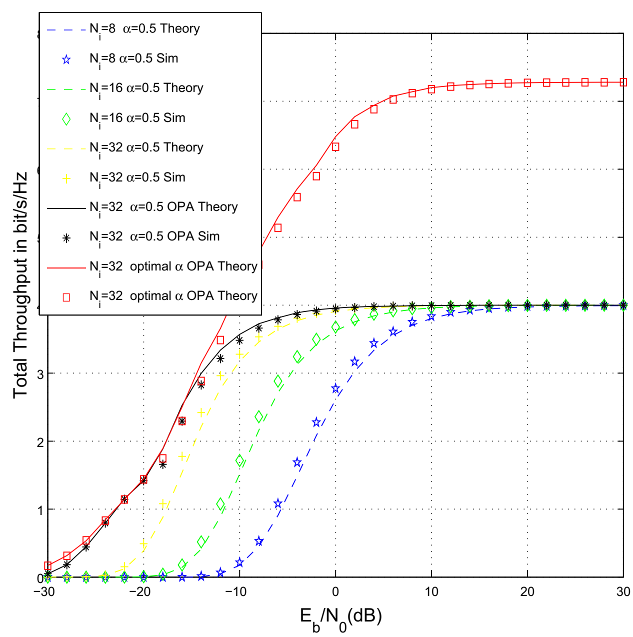

Fig. 6 Total throughput in the presence of 2 NOMA users for 16QAM modulation

The distances between P_S and users U_1, U_2 and U_3 are 2, 2.5 and 3. The other parameters are the same as Figs. 2 and 3. When the number of reflector per user is $N_i = 32$ we obtained 6,12 dB gain with respect to $N_i = 16, 8$. When powers allocated to NOMA users are optimized we obtained up to 5 dB gain with respect to $P_1 = 0.2$, $P_2 = 0.3$ and $P_3 = 0.5$. When harvesting duration α is optimized as well as the allocated NOMA powers, we obtained the largest throughput.

Figure 8 depicts the throughput of NOMA and orthogonal multiple access (OMA) when IRS are used and without IRS [20,21]. The parameters are the same as Figs. 2 and 3. When $N_i = 8, 32$ reflectors per user are employed, we obtained 24 and 41 dB gain with respect to NOMA with adaptive transmit power, energy harvesting and without IRS [20,21]. OMA without IRS offers a better throughput than NOMA without IRS at low average SNR per bit. At high average SNR per

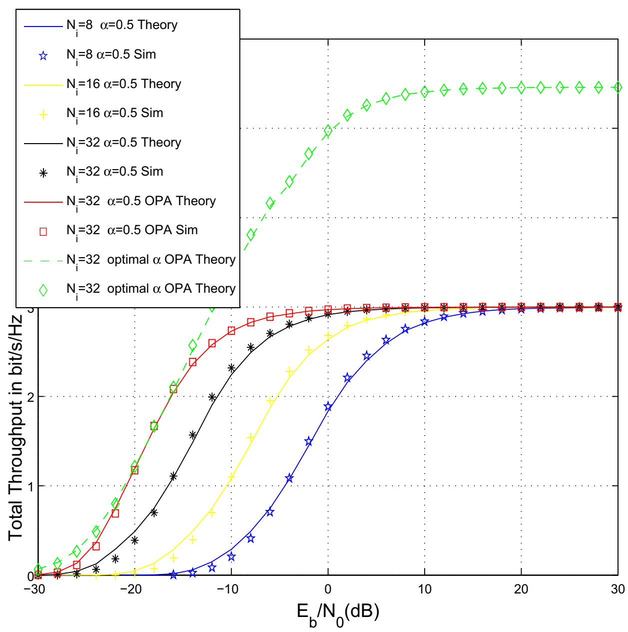

Fig. 7 Total throughput in the presence of 3 NOMA users for QPSK modulation

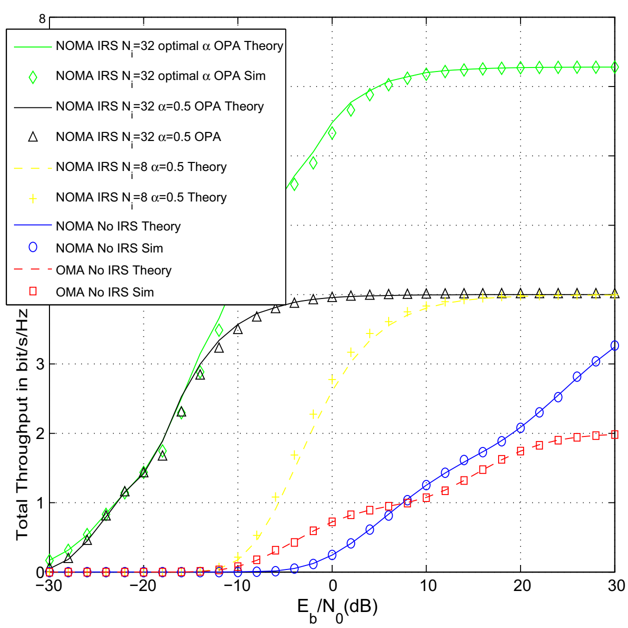

Fig. 8 Total throughput of OMA and NOMA with and without IRS in the presence of 2 NOMA users for 16QAM modulation

bit, NOMA without IRS offers a better throughput than OMA without IRS.

Figure 9 shows the effects of interference $T = 1, 5$ threshold on secondary throughput for the same parameters as Figs. 2 and 3. The number of reflectors per user is $N_i = 8$. When T increases, S_S can increase its power since there is less interference constraints and the throughput increases.

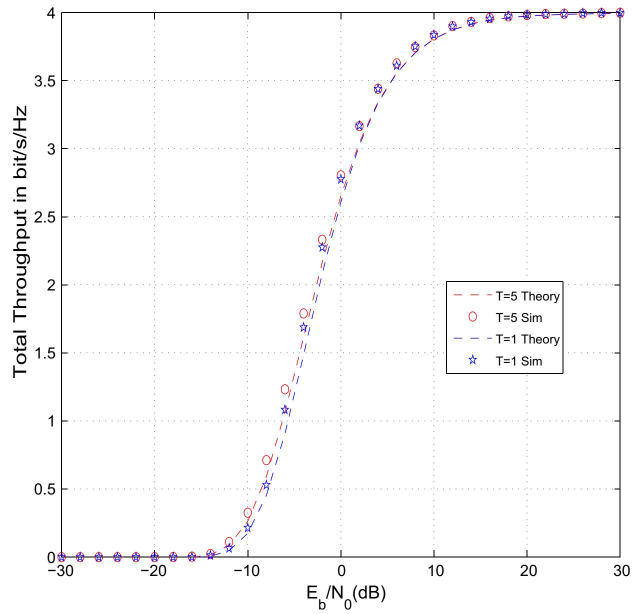

Fig. 9 Effects of interference threshold on total throughput for QPSK modulation and two users: $\alpha = 0.5$

6 Conclusion and perspectives

In this paper, we computed the throughput of cognitive radio networks using NOMA and intelligent reflecting surfaces where the secondary source harvests energy from the received RF signal from node A. Besides, the secondary source adapts its power to reduce the generated interference at primary destination. The secondary source transmits a linear combination of K symbols dedicated to K secondary users. The transmitted signal is reflected by a set I_i of reflectors dedicated to user U_i so that all reflections are in phase at U_i. When $N_i = 8, 32$ reflectors per user are employed, we obtained 24 and 41 dB gain with respect to NOMA with adaptive transmit power, energy harvesting and without IRS [20,21]. We also optimized NOMA powers and the harvesting duration. As a perspective, we can consider other source of energy such as wind and solar.

References

1. Basar, E., Di Renzo, M., De Rosny, J., Debbah, M., Alouini, M.-S., Zhang, R.: Wireless Communications Through Reconfigurable Intelligent Surfaces. IEEE Access **7**, 2019 (2019)
2. Zhang, H., Di, B., Song, L., Han, Z.: Reconfigurable intelligent surfaces assisted communications with limited phase shifts: how many phase shifts are enough? IEEE Trans. Veh. Technol. **69**(4), 4498–4502 (2020)
3. Di Renzo, M.: 6G wireless: wireless networks empowered by reconfigurable intelligent surfaces. In: 2019 25th Asia-Pacific Conference on Communications (APCC)

4. Basar, E.: Reconfigurable intelligent surface-based index modulation: a new beyond MIMO paradigm for 6G. IEEE Trans. Commun. **68**, 3187–3196 (2020)
5. Wu, Q., Zhang, R.: Towards smart and reconfigurable environment: intelligent reflecting surface aided wireless network. IEEE Commun. Mag. **58**(1), 106–112 (2020)
6. Huang, C., Zappone, A., Alexandropoulos, G.C., Debbah, M., Yuen, C.: Reconfigurable intelligent surfaces for energy efficiency in wireless communication. IEEE Trans. Wirel. Commun. **18**(8), 4157–4170 (2019)
7. Alexandropoulos, G.C., Vlachos, E.: A hardware architecture for reconfigurable intelligent surfaces with minimal active elements for explicit channel estimation. In: ICASSP 2020 - 2020 IEEE International Conference on Acoustics, Speech and Signal Processing (ICASSP) (2020)
8. Guo, H., Liang, Y.-C., Chen, J., Larsson, E.G.: Weighted sum-rate maximization for reconfigurable intelligent surface aided wireless networks. IEEE Trans. Wirel. Commun. **19**, 3064–3076 (2020)
9. Thirumavalavan, V.C., Jayaraman, T.S.: BER analysis of reconfigurable intelligent surface assisted downlink power domain NOMA system. In: 2020 International Conference on COMmunication Systems and NETworkS (COMSNETS) (2020)
10. Pradhan, C., Li, A., Song, L., Vucetic, B., Li, Y.: Hybrid precoding design for reconfigurable intelligent surface aided mmWave communication systems. IEEE Wirel. Commun. Lett. **9**, 1041–1045 (2020)
11. Ying, K., Gao, Z., Lyu, S., Wu, Y., Wang, H., Alouini, M.-S.: GMD-based hybrid beamforming for large reconfigurable intelligent surface assisted millimeter-wave massive MIMO. IEEE Access **8**, 109530–19539 (2020)
12. Yang, L., Guo, W., Ansari, I.S.: Mixed dual-hop FSO-RF communication systems through reconfigurable intelligent surface. IEEE Commun. Lett. **24**, 1558–1562 (2020)
13. Di, B., Zhang, H., Li, L., Song, L., Li, Y., Han, Z.: Practical hybrid beamforming with finite-resolution phase shifters for reconfigurable intelligent surface based multi-user communications. IEEE Trans. Veh. Technol. **69**(4), 4565–4570 (2020)
14. Nadeem, Q.-A., Kammoun, A., Chaaban, A., Debbah, M., Alouini, M.-S.: Asymptotic max-min SINR analysis of reconfigurable intelligent surface assisted MISO systems. IEEE Trans. Wirel. Commun. **19**, 7748–7764 (2020)
15. Zhao, W., Wang, G., Atapattu, S., Tsiftsis, T.A., Tellambura, C.: Is backscatter link stronger than direct link in reconfigurable intelligent surface-assisted system? IEEE Commun. Lett. **24**, 1342–1346 (2020)
16. Li, S., Duo, B., Yuan, X., Liang, Y.-C., Di Renzo, M.: Reconfigurable intelligent surface assisted UAV communication: joint trajectory design and passive beamforming. IEEE Wirel. Commun. Lett. **9**, 716–720 (2020)
17. Dai, L., Wang, B., Wang, M., Yang, X., Tan, J., Bi, S., Xu, S., Yang, F., Chen, Z., Di Renzo, M., Chae, C.-B., Hanzo, L.: Reconfigurable intelligent surface-based wireless communications: antenna design, prototyping, and experimental results. IEEE Access **8**, 45913–45923 (2020)
18. Hua, S., Shi, Y.: Reconfigurable intelligent surface for green edge inference in machine learning. In: 2019 IEEE Globecom Workshops (GC Wkshps) (2019)
19. Huang, C., Alexandropoulos, G.C., Yuen, C., Debbah, M.: Indoor signal focusing with deep learning designed reconfigurable intelligent surfaces. In: 2019 IEEE 20th International Workshop on Signal Processing Advances in Wireless Communications (SPAWC) (2019)
20. Alhamad, R., Boujemaa, H.: Throughput enhancement of cognitive radio networks-nonorthogonal multiple access with energy harvesting and adaptive transmit power. Trans. Emerg. Telecommun. Technol. **31**(8), e3980 (2020)
21. Alhamad, R., Boujemaa, H.: Optimal power allocation for CRN-NOMA systems with adaptive transmit power. Signal Image Video Process. **14**(7), 1327–1334 (2020)
22. Alhamad, R., Boujemaa, H.: Non orthogonal multiple access for MC-CDMA systems. Signal Image Video Process. (2021, Submitted to)
23. Xi, Y., Burr, A., Wei, J.B., Grace, D.: A general upper bound to evaluate packet error rate over quasi-static fading channels. IEEE Trans. Wirel. Commun. **10**(5), 1373–1377 (2011)
24. Proakis, J.: Digital Communications, 5th edn. Mac Graw-Hill, New York (2007)